Wideband mHEMT MMIC Low Noise Amplifier for the Next Generation Very Large Array Radio Telescope

Nianhua Jiang*
Herzberg Astronomy & Astrophysics Research Centre, National Research Council Canada
Victoria, BC, Canada
nianhua.jiang@nrc-cnrc.gc.ca

Alireza Seyfollahi
Qualcomm Inc
Santa Clara, California, USA
aseyfoll@qti.qualcomm.com

Deisy Formiga Mamedes
Herzberg Astronomy & Astrophysics Research Centre, National Research Council Canada
Victoria, BC, Canada
deisy.mamedes@nrc-cnrc.gc.ca

Doug Henke
Herzberg Astronomy & Astrophysics Research Centre, National Research Council Canada
Victoria, BC, Canada
douglas.henke@nrc-cnrc.gc.ca

Sara Salem Hesari
Herzberg Astronomy & Astrophysics Research Centre, National Research Council Canada
Victoria, BC, Canada
sara.salemhesari@nrc-cnrc.gc.ca

Adam Densmore
Herzberg Astronomy & Astrophysics Research Centre, National Research Council Canada
Victoria, BC, Canada
adam.densmore@nrc-cnrc.gc.ca

Lewis B.G. Knee
Herzberg Astronomy & Astrophysics Research Centre, National Research Council Canada
Victoria, BC, Canada
lewis.knee@nrc-cnrc.gc.ca

Philip Dindo
Central Development Laboratory National Radio Astronomy Observatory
Charlottesville, VA, USA
pdindo@nrao.edu

Pat Niranjanan
Herzberg Astronomy & Astrophysics Research Centre, National Research Council Canada
Victoria, BC, Canada
pat.niranjanan@nrc-cnrc.gc.ca

Dominic Garcia
Herzberg Astronomy & Astrophysics Research Centre, National Research Council Canada
Victoria, BC, Canada
dominic.garcia@nrc-cnrc.gc.ca

Jens Bornemann
Dept. of Electrical & Computer Engineering, University of Victoria
Victoria, BC, Canada
jbornema@ece.uvic.ca

***Abstract*—A wideband (28 - 52 GHz) monolithic microwave integrated circuit (MMIC) low noise amplifier (LNA) has been developed for the Band 5 receiver of the next generation Very Large Array (ngVLA) radio observatory. The MMIC LNA is designed on a 5-stage common source transistor configuration and double-resonance network for wideband input impedance and low noise matching based on a 70-nm GaAs metamorphic high electron mobility transistor (mHEMT). Two LNA chassis designs (coaxial connectors or waveguide system) are presented as alternatives for receiver integration. The fabricated MMIC LNA chips have been packaged and measured in two different packaging formats: (1) a chassis with a 50 Ω coaxial glass bead to microstrip transition, and (2) a chassis employing a WR-22 waveguide to microstrip probe transition. The measured results show that the waveguide port LNA achieved 1.6 dB average noise figure and 1.2 dB minimum noise figure; the LNA packaged with coaxial connector chassis had 2.2 dB average noise figure and 1.5 dB minimum noise figure, and 33 dB average gain from 28 to 52 GHz. The LNA design demonstrates wideband performance, low noise figure, high gain, and compact chip size. They can be applied to wideband receivers for radio astronomy and broadband communication applications.**

Keywords—low noise amplifier, LNA, GaAs mHEMT, millimeter wave, monolithic microwave integrated circuit, MMIC, RF package design, radio astronomy, next generation very large array, ngVLA.

I. INTRODUCTION

Radio telescope arrays consist of multiple radio antennas linked together to function as a single, massive instrument. They form an interferometric telescope to combine signals, providing larger collecting area and far higher angular resolution than a single dish. The overall sensitivity of telescope arrays can be increased by either increasing the number of antennas or reducing the noise introduced by the receiver components. The former directly increases the cost of construction and maintenance of the telescopes as well as the complexity of the system architecture. However, the latter can be achieved by designing lower noise components, specifically the noise and gain of the LNAs that dominate the overall receiver sensitivity. This allows for overall performance improvement without major increases in the telescope construction and maintenance cost.

The next generation Very Large Array (ngVLA) radio telescope was recommended for a development program and possible future construction in the US National Academies Astro2020 study [1] and has been recommended by the Canadian Astronomical Society's Long Range Plan 2020 [2] for

979-8-3195-0848-5/26/$31.00 ©2026 IEEE

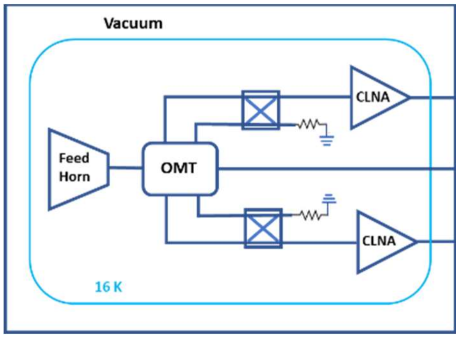

Fig. 1. ngVLA Band 5 receiver block diagram.

Canadian participation. The ngVLA telescope will have 6 frequency bands covering 1.2 to 116 GHz, comprised of 244 antennas of 18-meter diameter and 19 antennas of 6-meter diameter and a maximum baseline of 8860 kms [3]. The ngVLA offers state-of-the-art technology to provide scientists with the highest sensitivity and angular resolution and complementing the other two major radio telescopes: the Atacama Large Millimeter/submillimeter Array (ALMA) [4] and the Square Kilometre Array (SKA) [5]. Main science goals for the ngVLA include the study of the formation of solar system analogues on terrestrial scales and probing the initial conditions for planetary systems.

The ngVLA Band 5 receivers are cryogenically cooled to 16 K to reduce the thermal noise. The receiver noise temperature requirement is < 25 K (NF = 0.36 dB) within the Band 5 frequency range 30.5 to 50.5 GHz. A simplified system diagram of the Band 5 receiver is shown in Figure 1. The weak signals collected by the antenna are fed to a corrugated horn. The orthomode transducer (OMT) separates the RF signals into two orthogonal linearly polarized channels. As shown in Figure 1, each polarization channel needs two LNAs, one cryogenic LNA (CLNA) at 16 K, and a second (warm) LNA operating at room temperature. The cryogenic LNA significantly reduces the thermal noise contribution and provides > 30 dB gain. The warm LNA further increases the signal level without degrading the noise performance and provides higher signal power for frequency down conversion and digitization in the signal downstream [6].

In this paper we present the development of the warm LNA operated at room temperature. The circuit design methodology and packaging chassis design are discussed for wideband, low reflection, low noise matching, and reliable performance achieving the ngVLA Band 5 requirements by using a commercially available mHEMT MMIC foundry. The goal is to achieve a flat gain > 30 dB, S11 and S22 < -10 dB with the average noise figure ⩽ 2.5 dB from 30.5 to 50.5 GHz in a packaged LNA module. The transistor technology used in this process is OMMIC's 70 nm gate length process that offers a cut-off frequency (f_t) of 300 GHz. The double mushroom structure of the gate electrode supports a very high transconductance of 1600 mS/mm. The process offers a minimum noise figure of 0.55 dB at 30 GHz with about 130 mA/mm current density. The maximum stable gain is 17 dB at this low noise bias condition. This process also offers high quality MIM capacitors and thin film resistors [7].

II. Input and Low Noise Design

Simultaneous impedance matching for both 50 Ω input and minimum noise is the major challenge in the design of wideband low noise amplifiers. For high gain and low noise applications, a common source amplifier is preferred. A single stage common source amplifier with an inductance degeneration at source is shown in Figure 2. Its bandwidth is inversely proportional to the quality factor of the L_g-C_{gs} resonance. In order to extend the noise matching beyond the resonance bandwidth, adding a secondary resonance can allow for widening the bandwidth without compromising noise performance. This can be achieved by adjusting the capacitance of the large coupling capacitor (C_s) and replacing a large gate bias resistor (R_g) by an inductor (L_p) so they resonate at the lowest frequency of the band of interest. The L_g is designed to resonate with the transistor's C_{gs} at the upper side of the band of interest.

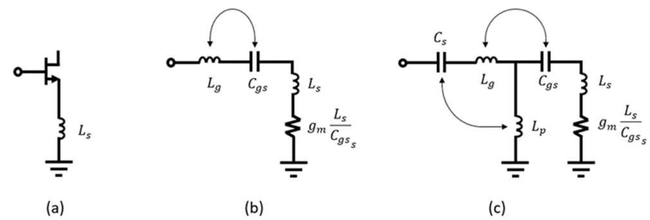

Fig. 2. (a) Common source transistor with source degeneration. (b) A single-resonance (L_g-C_{gs}) input matching network. (c) Double-resonance matching network (L_g-C_{gs} and C_s-L_p).

This configuration allows for simultaneous wideband low noise and input reflection matching. Figure 3 shows the comparison between a single-resonance and double-resonance matching network for a 4×25 µm transistor that is loaded with L_d = 80 pH inductor at its drain to peak the gain at 40 GHz. Figure 3(a) shows a common source amplifier where the decoupling capacitor (C_s) and the shunt inductor (L_p) are used to create a resonance at lower frequency and widen the input matching bandwidth. Figure 3(b) shows the comparison of input reflections between a single-resonance and double-resonance matching network.

Another benefit is the possibility of gain improvement and noise matching over a wider bandwidth. The amplifier with double-resonance at the input is able to achieve a noise figure very close to the minimum noise figure of the transistor for the wider frequency as depicted in Figure 3(c). Moreover, higher gain (about 3 dB) over wider bandwidth is realized in Figure 3(d) due to the small inductance degeneration used for input matching.

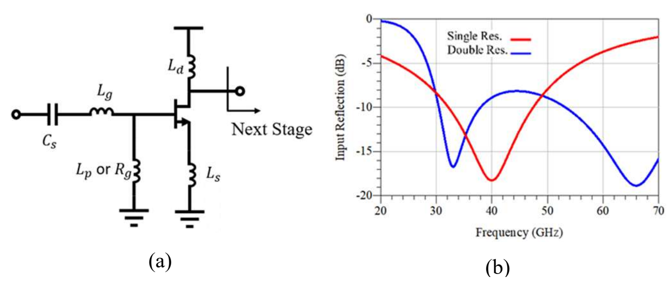

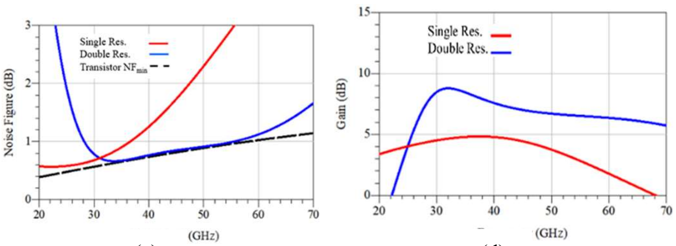

(c) (d)

Fig. 3. Comparison of single-resonance and double-resonance network. (a) A common source transistor with double-resonance circuit and inductance degeneration at source. (b) Simulation results of input reflections. (c) Simulation noise figures. (d) Simulation gains.

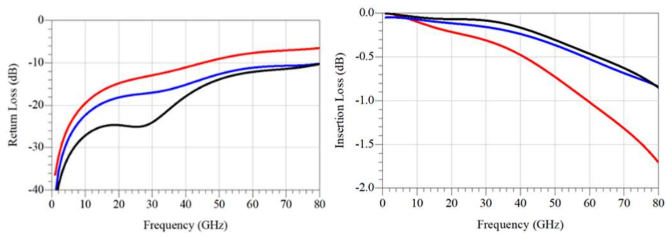

(a) (b)

Fig. 4. The simulated return loss (a) and insertion loss (b) of a 50 Ω microstrip-to-chip bond using a 15 mil long gold wire with 1 mil diameter, including single bonding wire with a standard bond pad (red), double bonding wires with a standard bond pad size (blue), and double bonding wires with a large bond pad size to compensates the bonding wires inductance (black).

The circuit design is still susceptible to the packaging chassis and the effect of the bonding wires, even with a wire length as short as 15 mil at 50 GHz. Therefore, a co-design approach including MMIC and LNA packaging is employed to take account of the parasitics from the interconnections at the input and output of the chip. The inductance of bonding wires can be compensated only up to a certain degree; therefore, the input impedance and noise matching is more challenging at high frequencies. Using double bonding wires can reduce the overall inductance of the connection and mitigate the matching network design. To further reduce the effect of the bonding wires, the bonding pad size as a capacitance can be optimized to compensate the effect of the wire inductance at high frequencies.

Figure 4 shows the EM simulation results for three case studies. As shown in Figure 4(a) the single bonding wire cannot achieve S11 ≤ -10 dB at 50 GHz; the double bonding wires improve S11 by -4 dB. In the case of double bonding wires plus a large bonding pad to compensate the wire inductance, the bonding wires and bonding pad form an *L-C* loop to add a resonance at about 28 GHz, and reduce S11 further to -14 dB up to 50 GHz, thus extending the bandwidth. In addition, the insertion loss of bonding wires is also reduced to 0.35 dB from 0.75 dB at 50 GHz as in Figure 4(b).

III. MMIC LNA SIMULATION

In order to achieve more than 30 dB gain and a bandwidth of 30.5 to 50.5 GHz, five transistor stages were used. Figure 5 shows the schematic of a cascaded common-source five transistor LNA as in the previous discussion. The drain

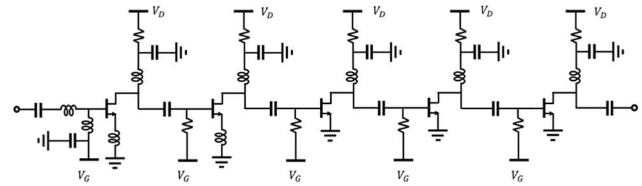

Fig. 5. Schematic diagram of the 5-stage GaAs mHEMT MMIC LNA.

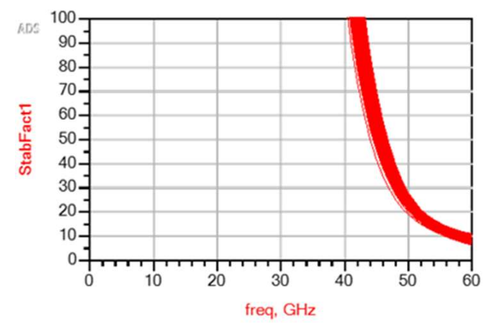

Fig. 6. The stability k factors of LNA were plotted with Monte Carlo yield analysis on component tolerance.

inductance of each stage is tuned to resonate with the drain capacitance at different frequencies, therefore the five stages can cover 28 to 52 GHz. The minimum noise figure of the transistors depends on the drain current density. The optimum bias for low noise performance is at 100-200 mA/mm as reported in [6]. Thus, all the devices are biased at around 100 mA/mm for low noise and low power operation of the mHEMTs. This corresponds to about 0.55 dB and 0.8 dB minimum noise figure of the transistors at 30 GHz and 50 GHz, respectively. As discussed earlier, the double-resonance network provides wideband input impedance matching, and the source degeneration in the first and second stage facilitates the low noise matching [8, 9]. This combination of techniques can achieve an optimum trade-off between S11 and noise performance.

The gate voltage is applied via the shunt inductor to the first stage and via large resistors of 2 kΩ to the rest of the transistors. Each stage's drain inductance is implemented by microstrip stubs that are terminated using a shunt capacitor on-chip. A small resistor of 5 Ω in the drain loop is used to help achieving unconditional stability. The LNA circuit stability was investigated with Monte Carlo yield analysis on component tolerance. As shown in Figure 6, the stability k factor of LNA is much higher than 1 up to 60 GHz. These resistors have minimal effect on noise performance. Single layer off-chip capacitors are used for all of the DC bias connections.

The designed circuit schematic in Figure 5 was optimized and converted to a MMIC layout for electromagnetic simulation and final tuning of the circuit layout. The simulated S-parameters of the MMIC LNA are plotted in Figure 7(a). This MMIC chip design achieves a wideband of 28 to 52 GHz with more than 30 dB flat gain, and better than -10 dB in S11 and S22. The simulated noise figure of the chip shown in Figure 7(b) varies from 1 to 1.25 dB over 28 to 52 GHz. The 5-stage MMIC LNA layout is implemented in a chip of 3x1 mm^2 on a 100 µm

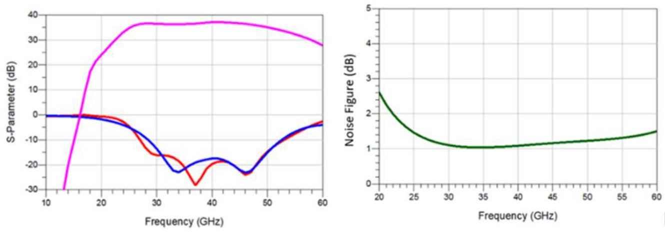

(a) (b)

Fig. 7. (a) Simulated gain, S11, and S22 of the MMIC LNA chip.
(b) Simulated noise figure of the MMIC LNA chip.

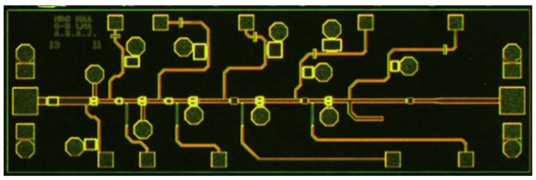

Fig. 8. Microphotograph of the fabricated GaAs mHEMT LNA

GaAs substrate. A microphotograph of the fabricated MMIC chip is shown in Figure 8.

IV. LNA Chassis Design

Providing an alternative for receiver integration of coaxial cable or a waveguide system, two different chassis were designed and fabricated. One design uses a coaxial interface where a V-type coaxial connector is transitioned to a microstrip via a 50 Ω coaxial glass bead. The microstrip is bonded to the MMIC chip pads using 1 mil gold wires at input and output. The second chassis was designed with WR-22 waveguide ports, in which a quartz microstrip probe converts the TE_{10} mode from the WR-22 waveguide into a microstrip line mode. The microstrip probe is wire-bonded to the MMIC chip pads at input and output. This waveguide design provides low input reflection and low insertion loss for integration with the orthomode transducer in the receiver module.

Packaging chassis design is critical for MMIC LNAs to reliably operate at 50 GHz. The chassis has to prevent unwanted higher modes excited from all of the discontinuities such as bonding wires, coaxial to microstrip transitions, waveguide to microstrip transitions, MMIC circuit, and off-chip components. The higher mode cut-off frequency for the single mode operation (microstrip line mode) is mostly dependent on the width of the channel to accommodate the MMIC chip inside the chassis. When the higher mode cut-off frequencies fall within the operational frequency range, higher modes/cavity resonances will appear and the RF signal/energy will no longer be fully contained in the microstrip line and the MMIC chip. The LNA will behave like an oscillator and cause a drop in gain, an increase in noise, and signal distortion.

To make room for the MMIC chip and off-chip component placement and bonding wires, the channel should have sufficient width while keeping the higher mode cut-off frequency far above 50 GHz. Two rows of metal pillars are used to define the channel width as shown in Figure 9. The metal pillar gaps facilitate the layout of off-chip components and bonding wires for DC bias connections. The pillar size, pillar gap, and channel width must be optimized to suppress higher mode frequencies up to 60 GHz. In order to verify the chassis design and cavity mode cut-off frequency, all RF components, DC bias circuit, bonding wires, 50 Ω coaxial glass beads, microstrip lines, and the MMIC chip were included into the 3D model of the chassis. The 3D mode EM simulation verified that the chassis structure has a cavity mode cut-of frequency of 66 GHz as shown in Figure 10. This chassis design can be used for MMIC LNA packaging for operation up to 60 GHz.

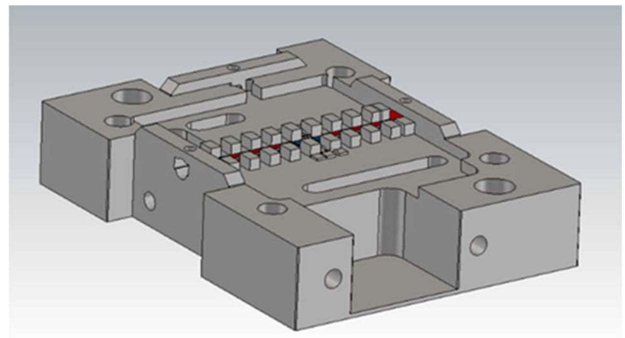

Fig. 9. Chassis 3D model with coaxial interface.

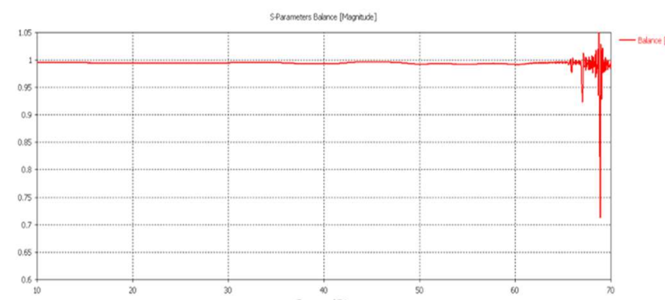

Fig. 10. EM simulated signal energy balance with all components and MMIC chip modeled in the chassis.

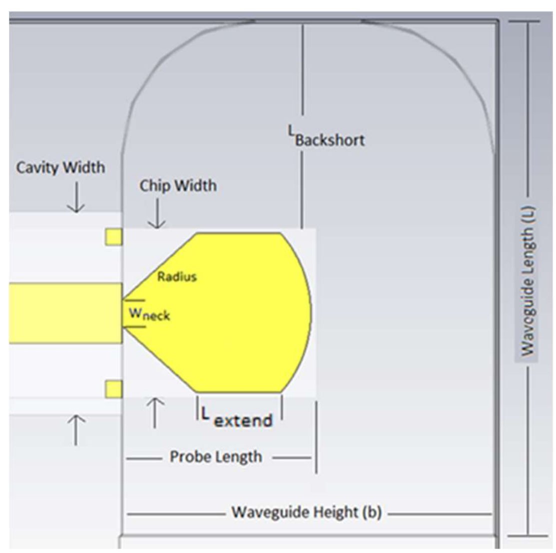

Fig. 11. Quartz microstrip probe for transition of WR-22 waveguide to 50 Ω microstrip.

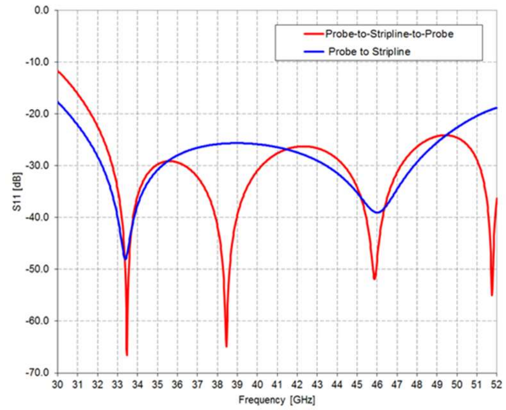

(a) Simulated reflection of microstrip probe

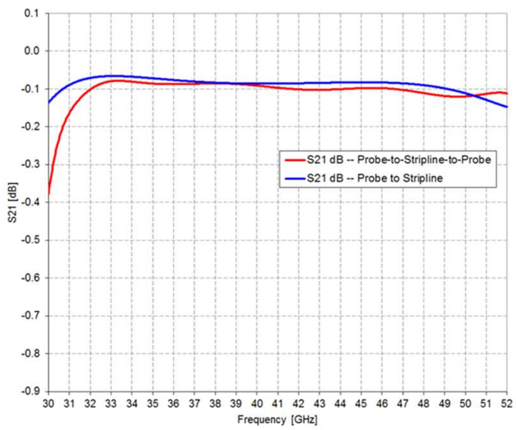

(b) Simulated insertion loss of microstrip probe

Fig. 12. Simulated performance of the transition from WR-22 waveguide to 50 Ω microstrip on a quartz substrate.

In the waveguide port chassis design, the transition of the 50 Ω glass bead to microstrip is replaced by a transition of WR-22 waveguide to a microstrip probe fabricated on a quartz substrate, as shown in Figure 11. The microstrip probe design is critical for the transition to achieve low reflections, low loss, and wideband operation. The performance of the single probe to microstrip and back-to-back two probes are plotted together as shown in Figure 12 [10]. This waveguide to microstrip transition achieves reflections far below -15 dB and 0.1 dB insertion loss between 30 to 50 GHz.

V. LNA Measurements

The fabricated MMIC LNA chips were installed into two LNA chassis for evaluation measurements and comparison. All off-chip passive components were assembled with silver epoxy or solder. Figure 13(a) shows the assembled LNA chip in the coaxial chassis. The microstrip at the MMIC chip input should be kept as short as possible to minimize the loss and added-in noise caused by the microstrip. The off-chip single layer capacitors are placed close to the chip to reduce the bonding wire length as much as possible. Figure 13(b) shows the coaxial chassis with V-type connectors and the Micro D-sub connector.

The measured S-parameters of the amplifier with coaxial interface are shown in Figure 14(a). The packaged LNA achieves 33 dB average gain over 28-52 GHz with input and output return loss better than 10 dB. This packaged coaxial LNA

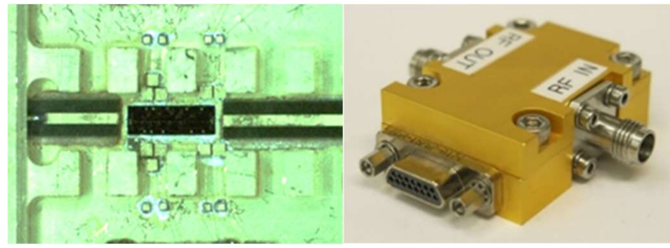

Fig. 13. (a) Inside view of the assembled coaxial chassis LNA. (b) Fully packaged LNA with V-type coaxial ports and Micro D-sub connector.

(a)

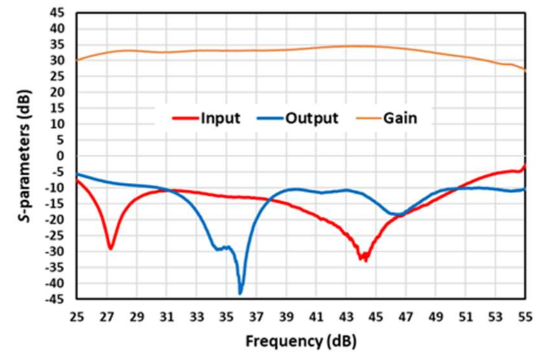

(b)

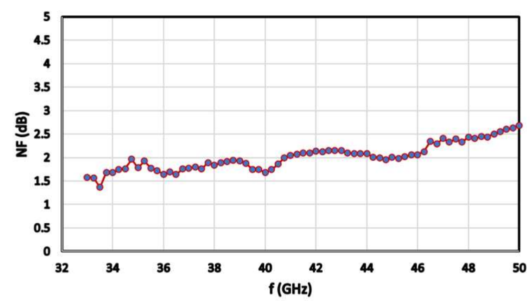

Fig. 14. (a) Measured S-parameters of the packaged LNA with coaxial chassis and V-type connectors. The LNA has 33 dB average gain and bandwidth of 28-52 GHz with input/output return loss better than 10 dB. (b) Measured noise figure.

module achieves 1.5 dB minimum noise and 2.2 dB average noise over the measurement bandwidth as plotted in Figure 14(b). The second MMIC LNA chip was packaged in the waveguide chassis shown in Figure 15. This chassis has WR-22 waveguide input and output ports. The measured S-parameters of the waveguide LNA module are shown in Figure 16. As WR-22 waveguide has a lowest order mode cut-off frequency close to 30 GHz, the reflection S11 and S22 parameters increases below 30 GHz. The input and output reflections are improved over the 30.5 to 50.5 GHz bandwidth of the coaxial LNA module. Furthermore, the waveguide LNA module achieves flat noise performance between 30 and 50 GHz, a lower average noise figure of 1.6 dB, and lower minimum noise figure of 1.2 dB than the coaxial LNA module.

VI. Summary

Wideband impedance and low noise matching techniques are presented for the design of a 28 to 52 GHz MMIC LNA. The packaging design of the MMIC LNA chassis is discussed. Two chassis, one with coaxial connectors and one with wave guide ports were designed and fabricated as alternatives for

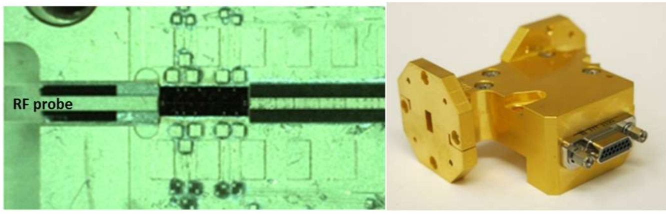

Fig. 15. (a) Inside view of assembled waveguide chassis LNA. (b) Fully packaged LNA with WR-22 ports and Micro D-sub connector.

(a)

(b)

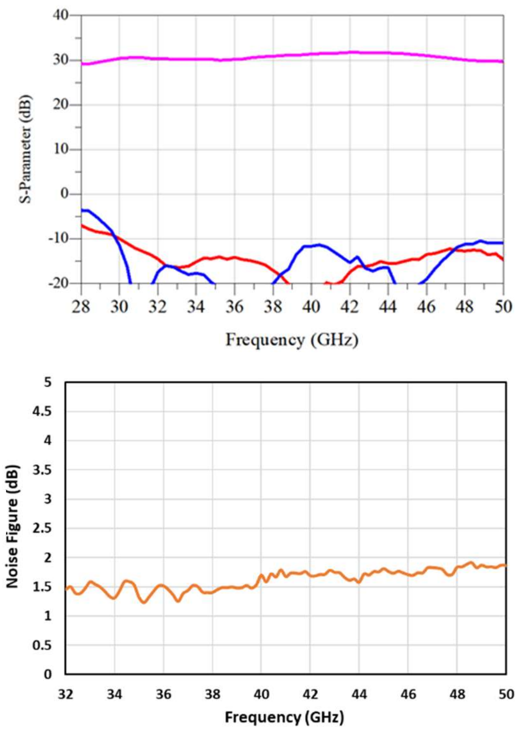

Fig. 16. (a) Measured S-parameters of the packaged LNA with WR-22 waveguide ports. The LNA has more than 30 dB gain and bandwidth of 30-50 GHz with input/output return loss better than 10 dB. (b) Measured noise figure.

receiver system integration. The two packaged LNA modules were characterized in the laboratory. The performance of these two LNAs meet the requirements of the warm amplifiers in the ngVLA Band 5 receiver system. Since the waveguide LNA module has a lower insertion loss from WR-22 to microstrip transition than the 50 Ω coaxial glass bead to microstrip transition, the waveguide LNA module achieves lower and flatter noise performance than the coaxial LNA module. Table I compares the performance of published LNAs for a similar frequency band with the LNA presented in this work. To the best of the authors' knowledge, the waveguide LNA achieves the lowest noise figure and highest gain reported for a packaged LNA based on mHEMT technology between 28 and 52 GHz. These wideband LNAs are also suitable for commercial and defense applications such as broadband communication, high quality and high-speed data streaming, 5G, and highly sensitive radar systems. This work demonstrates the wideband, low noise, and high gain performance of our MMIC LNA up to 52 GHz. We continue to develop cryogenic MMIC LNAs based on a similar design methodology for radio astronomy and other instrument applications.

TABLE I. PERFORMANCE LIST OF PUBLISHED LNAS AT SIMILAR FREQUENCY BAND WITH THE LNA PRESENTED IN THIS WORK

Ref.	Technology	Freq(GHz)	NF (dB)	S11 (dB)	Gain (dB)
[11]	pHEMT GaAs MMIC	27-45	3.1	-5	25
[12]	mHEMT GaAs MMIC	37-52	3.2	N.A	32.5
[13]	InP HEMT MMIC	24-40	1.6	-10	27
[14]	InP HEMT MMIC	18-43	1.9	-9	40
[15]	InP HEMT MMIC	32-52	1.8	-10	35
[16]	mHEMT GaAs MMIC	30-50	3.7	-13	20
[17]	mHEMT GaAs MMIC	33-50	1.8	-6	27
This work	mHEMT GaAs MMIC	30-50	1.6	-10	31.5

REFERENCES

[1] https://www.nationalacademies.org/read/26141/chapter/1

[2] https://casca.ca/wp-content/uploads/2021/05/LRP2020_final_EN.pdf

[3] http://ngvla.nrao.edu/

[4] https://www.almaobservatory.org/en/home/

[5] https://www.skao.int/en

[6] S. Salem Hesari, D. Henke, V. Reshetov, F. Jiang, A. Seyfollahi, L.B.G. Knee, L. Baker, J. Bornemann, and D. Chalmers, "Q-band receiver system design for the Canadian DVA-2 radio telescope," Proc. SPIE 11453 Astronomical Telescopes & Instrumentation, pp. 1-16, Digital Forum, Dec. 2020.

[7] D. Smith, G. Dambrine and J. Orlhac, "Industrial MHEMT Technologies for 80 - 220 GHz Applications," 2008 European Microwave Integrated Circuit Conference, 2008, pp. 214-217.

[8] Nianhua Jiang, Dominic Garcia, Pat Niranjanan, Mark Halman, Ivan Wevers "Extremely low noise UHF band amplifiers for square kilometer array" Proceedings of SPIE, Millimeter, Submillimeter, and Far-Infrared Detectors and Instrumentation for Astronomy VIII, Vol. 9914 991420-1, 2016.

[9] M. Fu, N. Jiang, J. Bornemann and Q. Feng, "Accurate Simulation of High-Gain MMIC Amplifiers with Microstrip-Type Transistors," in IEEE Transactions on Computer-Aided Design of Integrated Circuits and Systems, vol. 42, no. 1, pp. 16-26, Jan. 2023, doi: 10.1109/TCAD.2022.3174165

[10] Philip Dindo, "Simulation and Measurements of Waveguide to Strip-line Transition for ALMA Band1 Receiver", ALMA Band1 Kickoff meeting, Academia Sinica Institute of Astronomy and Astrophysics, Taiwan, June 12, 2012. Report Available on Request.

[11] S. H. Weng, W. C. Wang, H. Y. Chang, C. C. Chiong, and M.-T. Chen "An ultra low-power Q-band LNA with 50% bandwitdth in WIN GaAs 0.1-μm pHEMT process," *Proc. Asia-Pacific Microw. Conf*., 2013, pp. 713-715

[12] S.H. Weng, C.H. Lin, H.Y. Chang, and C.C. Chiong, "Q-band low noise amplifiers using a 0.15-μm MHEMT process for broadband communication and radio astronomy applications," IEEE MTT-S Int. Microw. Symp. Dig., June 2006, pp. 89-92.

[13] J. Schleeh, N. Wadefalk, P. Nilsson, J. P. Starski and J. Grahn, "Cryogenic Broadband Ultra-Low-Noise MMIC LNAs for Radio Astronomy Applications," in IEEE Transactions on Microwave Theory and Techniques, vol. 61, no. 2, pp. 871-877, Feb. 2013

[14] S. Masuda, T. Ohki and T. Hirose, "Very Compact High-Gain Broadband Low-Noise Amplifier in InP HEMT Technology," in *IEEE Transactions on Microwave Theory and Techniques*, vol. 54, no. 12, pp. 4565-4571, Dec. 2006

[15] E. Cha et al., "Two-Finger InP HEMT Design for Stable Cryogenic Operation of Ultra-Low-Noise Ka- and Q-Band

[16] S. Weng, W. Wang, H. Chang, C. Chiong and M. Chen, "A cryogenic 30–50 GHz balanced low noise amplifier using 0.15-μm MHEMT process for radio astronomy applications," *2012 IEEE International Symposium on Radio-Frequency Integration Technology (RFIT)*, 2012, pp. 177-179

[17] J. V. Terán Collantes, L. de la Fuente, B. Aja and E. Artal, "Cryogenic broadband Q-band MMIC low-noise amplifier," *2016 11th European Microwave Integrated Circuits Conference (EuMIC)*, 2016, pp. 77-80